Eur. Phys. J. C 49, 75–80 (2007)
DOI 10.1140/epjc/s10052-006-0099-0

THE EUROPEAN PHYSICAL JOURNAL C

Regular Article – Experimental Physics

Proton–proton, anti-proton–anti-proton, proton–anti-proton correlations in Au + Au collisions measured by STAR at RHIC

H.P. Gos[1,2,a] for the STAR collaboration

[1] Warsaw University of Technology, Faculty of Physics, Koszykowa 75, 00-662 Warsaw, Poland
[2] SUBATECH, Laboratoire de Physique Subatomique et des Technologies Associes, EMN-IN2P3, CNRS-Universite, 44307 Nantes, France

Received: 3 August 2006 /
Published online: 28 November 2006 –

Abstract. The analysis of two-particle correlations provides a powerful tool to study the properties of hot and dense matter created in heavy-ion collisions at ultra-relativistic energies. Applied to identical and non-identical hadron pairs, it makes the study of space-time evolution of the source in femtoscopic scale possible. Baryon femtoscopy allows extraction of the radii of produced sources which can be compared to those deduced from identical pion studies, providing complete information about the source characteristics. In this paper we present the correlation functions obtained for identical and non-identical baryon pairs of protons and anti-protons. The data were collected recently in Au + Au collisions at $\sqrt{s_{NN}} = 62$ GeV and $\sqrt{s_{NN}} = 200$ GeV by the STAR detector at the RHIC accelerator. We introduce corrections to the baryon–baryon correlations taking into account: residual correlations from weak decays, particle identification probability and the fraction of primary baryons. Finally we compare our results to theoretical predictions.

PACS. 25.75.-q; 25.75.Gz

1 Introduction

One of the four experiments conducted at relativistic heavy ion collider (RHIC) at Brookhaven National Laboratory (BNL) is the solenoidal tracker at RHIC (STAR). The STAR experiment was designed to measure the properties of hot and dense matter [1] created in heavy ion collisions at ultrarelativistic energies, where the transition from hadronic matter into partonic stage of the quark gluon plasma (QGP) was expected to occur. This gives the opportunity to study the formation of hadronic matter and the properties of interactions between hadrons. For six years, STAR detector has been collecting data from various nuclear collisions: $p+p$, $d+$Au, Au + Au and Cu + Cu at different energies: 22 GeV, 62 GeV, 130 GeV and 200 GeV. Differential data gathered with the same experimental setup provides the opportunity to study the bulk properties of nuclear systems that never before was possible with such accuracy.

The correlation effect is determined by the distance separating emission points in space and time and by the particles' relative momentum [6, 7] . By analyzing the momentum correlations it is possible to access information about source characteristics which cannot be measured directly. Identical baryon correlations reflect the properties of the quantum statistics (QS) [8, 9] and of the final state interactions (FSI) [10, 11]: Coulomb and strong. Non-identical baryon pairs are sensitive to the final state interactions only.

In this paper we present results for proton femtoscopy from Au + Au collisions at $\sqrt{s_{NN}} = 62$ GeV and $\sqrt{s_{NN}} = 200$ GeV. Two-proton correlations were intensively measured before at AGS (BNL) [2], SPS (CERN) [3, 4] and SIS (Darmstadt) [5] energies. However the STAR experiment has measured and fitted all three combinations of protons and anti-protons: $p-p$, $\overline{p}-\overline{p}$ and $p-\overline{p}$ for the first time creating a complex description of proton interferometry for various centralities and collision energies. In this paper we discuss detailed and important corrections, including residual correlations measured together with protons interactions, the fraction of pairs composed of primordial baryons, the particle identification probability and the tracks smearing being a consequence of a detector resolution. In order to fit experimental correlation functions we use CorrFit tool [12].

Our results are consistent with trends established using other particle species. The source sizes scale with event multiplicity, and the radii follow the $\frac{1}{\sqrt{m_{\mathrm{T}}}}$ systematic observed for pions, kaons and lambdas.

[a] e-mail: gos@if.pw.edu.pl

2 The formalism of two-particle correlations

We measure the correlations in the momentum difference variable $k^* = \frac{Q_{\rm inv}}{2} = \frac{1}{2}\sqrt{(p_1-p_2)^2-(E_1-E_2)^2}$. To measure the correlation effect we define the correlation function as a ratio: $C(k^*) = \frac{A(k^*)}{B(k^*)}$. We put pairs of particles coming from the same event (correlated) into numerator $A(k^*)$ and the pairs of particles from different events (not correlated) into denominator $B(k^*)$.

3 Experimental criteria on sample selection

Particles which come from Au + Au collisions at $\sqrt{s_{NN}} = 62\,\text{GeV}$ and $\sqrt{s_{NN}} = 200\,\text{GeV}$ are registered using the main STAR detector, the time projection chamber (TPC). 25 million minimum bias events are selected and divided into three centralities according to the percentage of total cross-section of the collision: central (0%–10%), midcentral (10%–30%), peripheral (30%–80%). Protons and anti-protons are measured in the rapidity window $|y| < 0.5$. Particles are selected using the energy loss in the detector ($\mathrm{d}E/\mathrm{d}x$). Protons and anti-protons are chosen in momentum range: $0.4\,\text{GeV/c} < p_{\rm T} < 0.8\,\text{GeV/c}$. Tracks are extrapolated to a primary vertex. If the shortest distance between track and the vertex exceeds 3 cm, the track is discarded, removing a significant fraction of non-primary track candidates. For identical particles ($p-p$ and $\overline{p}-\overline{p}$), track-splitting causes an artificial enhancement of the number of pairs at k^*. We remove splitted tracks candidates from both numerator and denominator of the correlation function. For identical and non-identical particles we remove candidates for merged tracks as well. The contribution of $\gamma \to e^+e^-$ conversions to $p-\overline{p}$ distribution is strongly suppressed using a pair topology cut. The background of the correlation function is constructed by mixing 10 different events according to similar Z-vertex orientation and multiplicity. Assuming that there is no correlation for non-primary pairs, the correlation functions are corrected for purity according to the (1)

$$C_{\rm true}(k^*) = \frac{C_{\rm measured}(k^*)-1}{\text{purity}(k^*)} + 1\,, \tag{1}$$

where $C_{\rm true}(k^*)$ means corrected and $C_{\rm measured}(k^*)$ is measured value of correlation function, $\text{purity}(k^*) = \text{Pair PID}(k^*)$ is the probability of being correctly registered (dependent on system) as a: $p-p$, $\overline{p}-\overline{p}$, $p-\overline{p}$ pair. The resolution effect of track smearing in the detector is taken into account as well.

4 The estimation of residual correlations

4.1 Basics of residual correlation effects

Previous measurements of baryon–baryon correlations [13–15] suggested two different source sizes dependent on whether or not the interaction has an annihilation channel. HBT radii deduced from identical baryon interferometry ($p-p$, $\overline{p}-\overline{p}$) were consistent for each cut on energy and centrality. However the source parameters derived from non-identical proton studies compared to ones concluded from identical proton femtoscopy were smaller in each centrality bin of both energies: $\sqrt{s_{NN}} = 62\,\text{GeV}$ and $\sqrt{s_{NN}} = 200\,\text{GeV}$. Those results were obtained without taking into account the effect of residual correlations due to baryons decaying into protons and anti-protons. From the experimental point of view, many secondary protons and anti-protons because are indistinguishable from primordial particles, their parent particles are not detected. Not taking this fact into consideration may lead to misinterpretation of the measured results, where instead of $p-p$ interaction the correlations between other particles (which decayed finally into proton) are observed. Two main weak decay channels of interest are considered here:

$$\Lambda \to p + \pi^- \tag{2}$$

$$\Sigma^+ \to p + \pi^0 \tag{3}$$

In fact, all residual correlations arising from decay channels which lead to proton (anti-proton) through hyperons are considered. In order to evaluate the effect of residual correlations occurring in proton femtoscopy, our analysis uses the Therminator (THERMal Heavy IoN GenerATOR) Monte Carlo event generator [16, 17]. The generator was designed to study particle production at SPS, RHIC and LHC energies. The program implements the thermal model of particle production with a single freeze-out. The geometry of the freeze-out hypersurface is chosen according to Cracow model [18–20]. The space-time emission point, as well as parent information is stored for each particle.

4.2 Combining contributions from several sources

The formula on experimentally measured proton–proton (and anti-proton–anti-proton) correlation is described by the (4):

$$\begin{aligned} CF_{\rm true}(k^*) &= CF_{p-p}(k^*)F_{p-p}(k^*) \\ &+ CF_{p-\Lambda}(k^*)F_{p-\Lambda}(k^*) + CF_{\Lambda-\Lambda}(k^*)F_{\Lambda-\Lambda}(k^*) \\ &+ CF_{p-\Sigma}(k^*)F_{p-\Sigma}(k^*) + CF_{\Sigma-\Sigma}(k^*)F_{\Sigma-\Sigma}(k^*) \\ &+ CF_{\Lambda-\Sigma}(k^*)F_{\Lambda-\Sigma}(k^*)\,, \end{aligned} \tag{4}$$

where $F_{x-y}(k^*)$ represents the fraction of measured $p-p$ pairs, where most primary parents were x and y. $CF_{x-y}(k^*)$ means the residual contribution of $x-y$ correlation. By $CF_{\rm true}(k^*)$ we mean the experimentally measured correlation function corrected for the particle identification probability (PID) purity.

The formula for the $p-\overline{p}$ system is a little more complicated as it contains all combinations of protons and anti-protons from 6 different groups. We do not describe here the mechanism of calculating the residual correlations existing in $p-\overline{p}$ system as it is similar to one for identical proton femtoscopy. The aim of this study is to estimate the pure $p-p$ correlation after removing from the measured observables the residual ones. In order to evaluate the

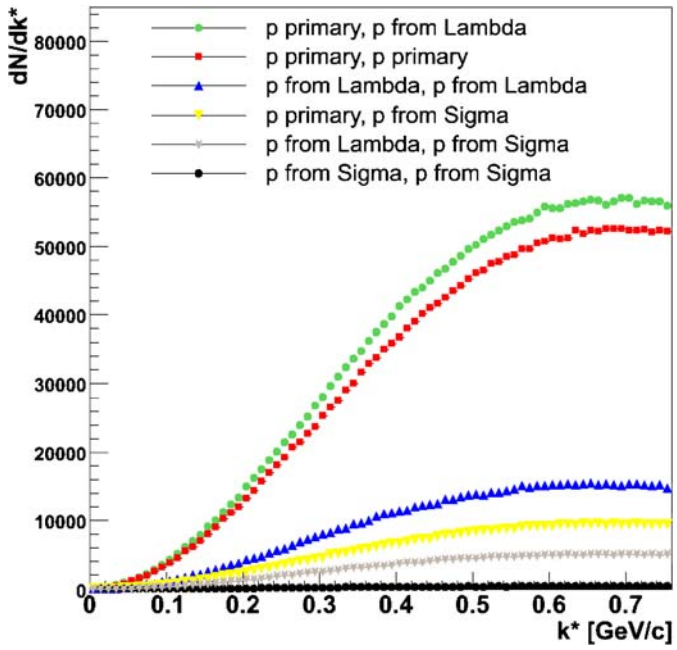

Fig. 1. Two-proton distributions of momentum differences in PRF

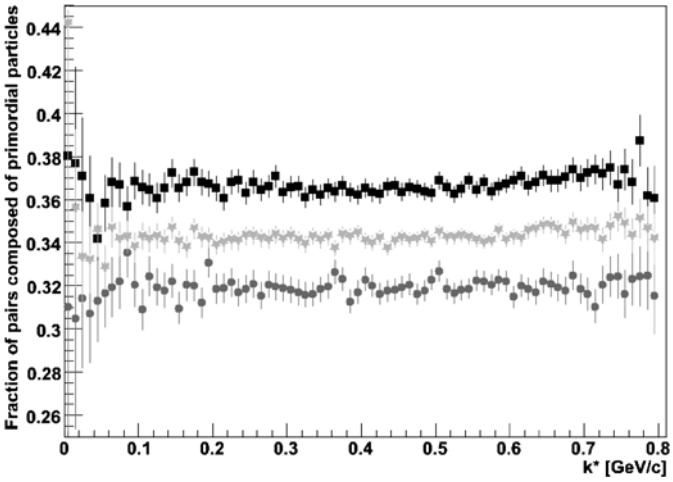

Fig. 2. The fraction of pairs composed of primordial particles: proton–proton (*black squares*), anti-proton–anti-proton (*dark gray circles*), proton–anti-proton (*bright stars*)

fractions $F_{x-y}(k^*)$ of each correlation, all protons are divided into three groups: primordial particles, protons coming from Λ hyperons and ones coming from decays of Σ^+ baryons. For all two-proton combinations, the k^* distributions are computed (Fig. 1). The dominant contribution comes from $p-\Lambda$ pairs for all k^* values, indicating that $p-\Lambda$ residual interaction strongly affects measured $p-p$ correlation. The presence of other types of residual correlations is much less significant.

The fraction of pure correlation is slightly k^* dependent function with the mean value from 0.31 (for the $\overline{p}-\overline{p}$ system) to 0.38 (for the $p-p$ system) due to $\overline{p}/p$ ratio smaller

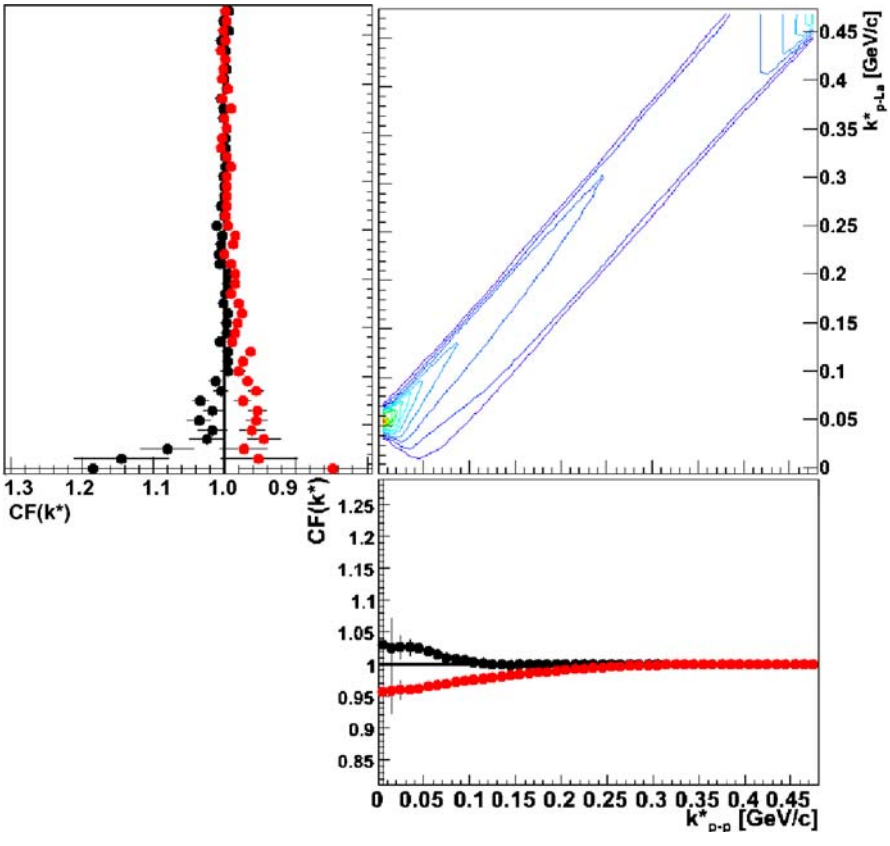

Fig. 3. Left-hand side of the top panel illustrates experimentally measured $p-\Lambda$ (*black marker*) and $\overline{p}-\Lambda$ (*gray marker*) correlation functions for central collisions. Right-hand side of the top panel shows kinematic dependencies $W(k^*_{p-p}, k^*_{p-\Lambda})$ of lambda decays, k^* of $p-\Lambda$ pairs versus k^* of $p-p$ pairs. Right-hand side of the bottom panel exhibits $p-\Lambda$ and $\overline{p}-\Lambda$ residual correlations reflected in correlation functions for $p-p, \overline{p}-\overline{p}$ (*black circles*) and $p-\overline{p}$ (*gray circles*)

than $\overline{\Lambda}/\Lambda$ ratio. The main week decay channels of protons and anti-protons are lambda and anti-lambda ones. The fraction of pure correlations is shown in Fig. 2.

4.3 Convolution of decay kinematics

The $p-\Lambda$ correlation function has been measured by STAR [15], as a function of $k^*_{p-\Lambda}$. However the argument of $CF_{p-\Lambda}$ in (4) is k^*_{p-p}, the relative momentum between two protons: in this case, one of the protons is the decay daughter of Λ. To calculate the $p-\Lambda$ contribution to the measured $p-p$ correlation function, the $p-\Lambda$ correlation function must be convoluted with the Λ decay kinematics. Figure 3 shows from which region of $k^*_{p-\Lambda}$ the $p-\Lambda$ residual correlation affect which range of k^*_{p-p} of experimentally measured $p-p$ correlation. For each value of k^*_{p-p}, the influence of $p-\Lambda$ correlation is computed (5) as a sum over all $k^*_{p-\Lambda}$ bins of experimentally measured $p-\Lambda$ correlation scaled by the factor from $W(k^*_{p-p}, k^*_{p-\Lambda})$ histogram. $p-\Lambda$ correlation cannot be corrected on purity as it contains the residual correlations derived from higher order decays.

$$CF_{p-\Lambda}\left(k^*_{p-p}\right) = \sum_{k^*_{p-\Lambda}} CF^{\mathrm{meas}}_{p-\Lambda}\left(k^*_{p-\Lambda}\right) W\left(k^*_{p-p}, k^*_{p-\Lambda}\right). \tag{5}$$

Residual correlations from $p-\Sigma^+$ and $\Sigma^+-\Sigma^+$ channels are assumed to arise only from Coulomb interactions for all systems in addition to quantum statistics for $\Sigma^+-\Sigma^+$. The (k^*_{p-p} and $k^*_{p-\Sigma^+}$), (k^*_{p-p} and $k_{\Sigma^+-\Sigma^+}$) kinematic dependencies of decay of Σ^+ hyperon are considered separately.

4.4 Effects on extracted length scales

The net effect of the purity and residual correlation corrections is shown in Fig. 4. All correlation functions shown are corrected for PID effects. A first estimate of the fraction of primary–primary proton pairs was 0.25. (i.e fraction of of primary protons 0.5); the correlation function corrected for this purity is shown. A better calculation of pair purity, discussed in Sect. 4.2 and Figs. 4 and 5, results in reduced correlation. Finally, the extracted correlation is further reduced when residual correlations are also corrected for.

Since the $\overline{p}-\Lambda$ correlation is much stronger and wider than $p-\Lambda$ one, the residual effects on the $p-\overline{p}$ system are more significant than those for $p-p$ system (see Fig. 3). This is clear in Fig. 5, where the effects of the various corrections on $p-\overline{p}$ are shown.

5 Gaussian source approximation

The correlation functions for Au + Au collisions at $\sqrt{s_{NN}} =$ 200 GeV for different centrality bins are shown in Figs. 6–8. For all systems the correlation effect decreases with increasing the centrality.

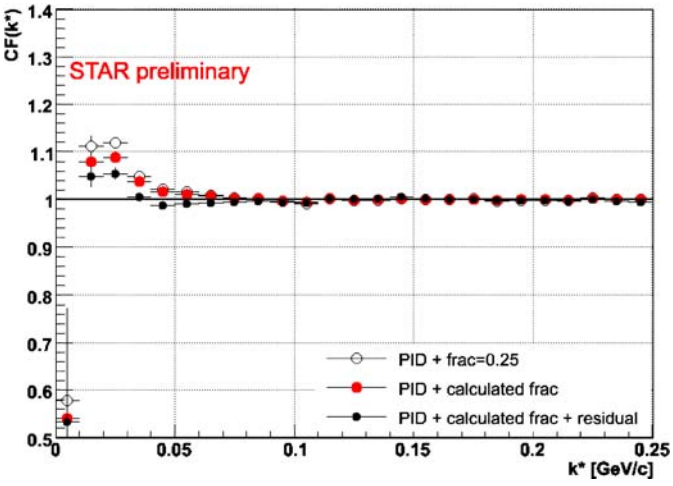

Fig. 4. Residual correlations in proton–proton system. The differences between *gray* (not corrected) and *black circles* (corrected on residual correlations) show the importance of residual correlation correction

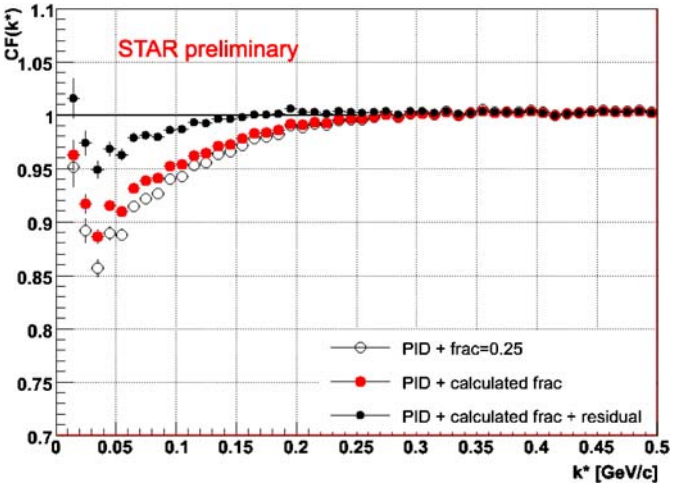

Fig. 5. Residual correlations in proton–anti-proton system. The differences between *gray* (not corrected) and *black* (corrected on residual correlations) show the importance of residual correlation correction

Using the Corrfit tool, we fit the correlation functions by convolving a Gaussian source in coordinate space with the squared wave functions of the two-particle system. This wave function includes coulomb and strong FSI, and quantum interference effects [6]. The extracted Gaussian radii are given in Tables 1 and 2 for $\sqrt{s_{NN}} = 200$ GeV and $\sqrt{s_{NN}} = 62$ GeV collisions respectively. Errors reported are statistical, but we estimate ~ 0.5 fm systematic errors due to uncertainties in the corrections. The approximate consistence for the different pair combinations, for all energies and centrality selections, gives us confidence in the stability of our results.

The extracted baryon interferometry radii for central collisions confirm hydrodynamical description of source evolution, where heavier particle species are expected to be emitted from smaller area. The system's collective ex-

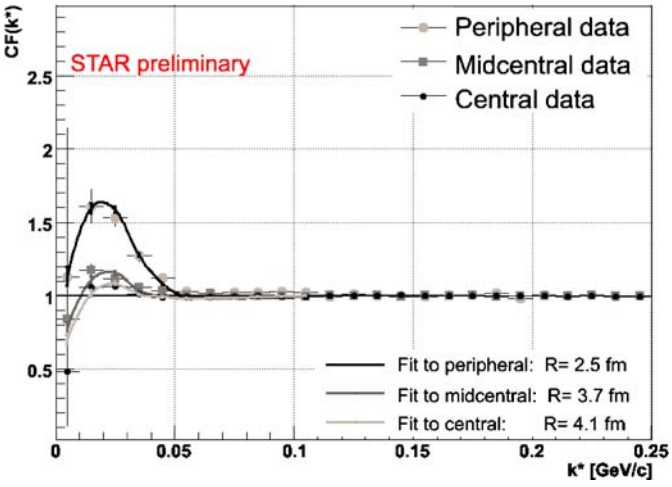

Fig. 6. Proton–proton correlation functions for $\sqrt{s_{NN}} =$ 200 GeV for three centralities: central, midcentral and peripheral collisions

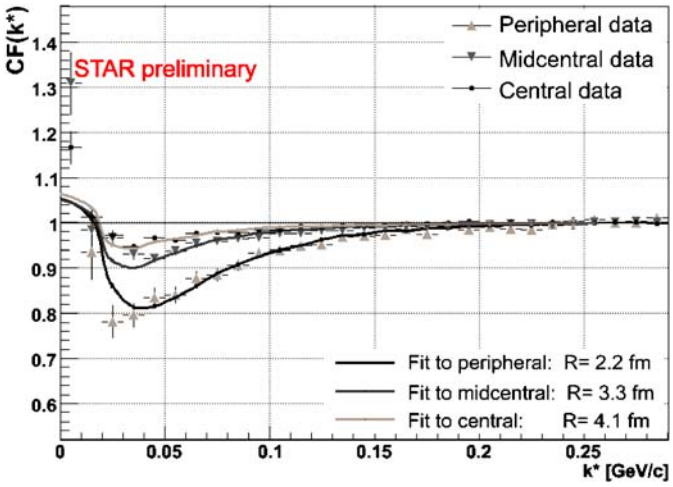

Fig. 8. Proton–anti-proton correlation functions for $\sqrt{s_{NN}} =$ 200 GeV for three centralities: central, midcentral and peripheral collisions

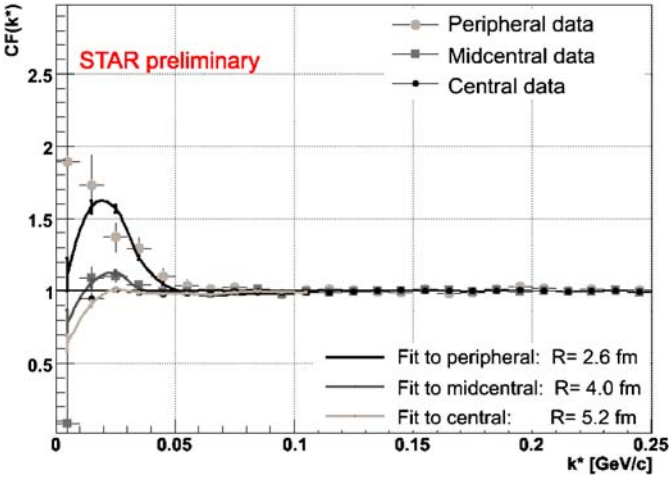

Fig. 7. Anti-proton–anti-proton correlation functions for $\sqrt{s_{NN}} = 200$ GeV for three centralities: central, midcentral and peripheral collisions

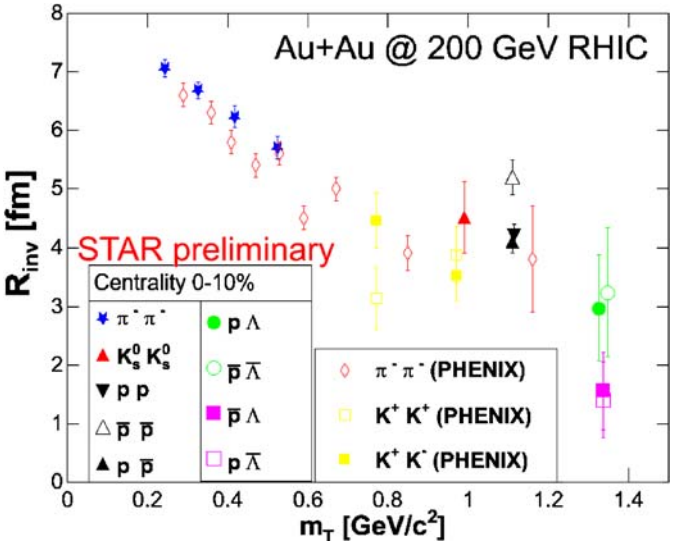

Fig. 9. $R_{\rm inv}$ values extracted from hadron femtoscopy at $\sqrt{s_{NN}} = 200$ GeV for 10% of central collisions

Table 1. Source sizes (in fm) for Au + Au collision at $\sqrt{s_{NN}} = 200$ GeV

Centrality	$p-p$	$\overline{p}-\overline{p}$	$p-\overline{p}$
Peripheral	$2.7^{+0.2}_{-0.2}$	$2.6^{+0.1}_{-0.2}$	$2.2^{+0.1}_{-0.1}$
Midcentral	$3.8^{+0.3}_{-0.3}$	$4.0^{+0.3}_{-0.2}$	$3.3^{+0.1}_{-0.1}$
Central	$4.2^{+0.2}_{-0.2}$	$5.2^{+0.3}_{-0.2}$	$4.1^{+0.2}_{-0.1}$

Table 2. Source sizes (in fm) for Au + Au collision at $\sqrt{s_{NN}} = 62$ GeV

Centrality	$p-p$	$p-\overline{p}$
Peripheral	$2.5^{+0.2}_{-0.3}$	$2.3^{+0.1}_{-0.1}$
Midcentral	$3.2^{+0.3}_{-0.2}$	$2.7^{+0.2}_{-0.2}$
Central	$4.2^{+0.4}_{-0.5}$	$3.5^{+0.2}_{-0.1}$

pansion produces such differences in length of homogeneity because massive particles (e.g. protons) are on average more pushed towards the edge of system than lighter ones (e.g. pions). In Fig. 9, the present results are seen to conform with the "universal" $m_{\rm T}$ systematics established with other particle species [7].

The nature of $({\rm d}N_{\rm ch}/{\rm d}\eta)^{1/3}$ scaling ($dN_{\rm ch}$-number of charge particles) of HBT radii, seen for the first time in pion interferometry [21], is observed also in proton femtoscopy. Studying such relations is motivated by connection $({\rm d}N_{\rm ch}/{\rm d}\eta)^{1/3}$ dependencies to the final state geometry through particle density at freeze-out. The Fig. 9

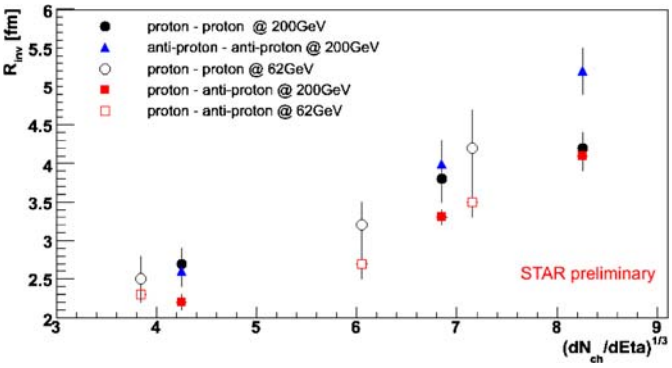

Fig. 10. $(\mathrm{d}N_{\mathrm{ch}}/\mathrm{d}\eta)^{1/3}$ scaling of source sizes from proton femtoscopy at $\sqrt{s_{NN}} = 62$ GeV and $\sqrt{s_{NN}} = 200$ GeV

presents such scaling for R_{inv} source sizes extracted from $p-p$, $\overline{p}-\overline{p}$ and $p-\overline{p}$ at $\sqrt{s_{NN}} = 62$ GeV and $\sqrt{s_{NN}} = 200$ GeV energies. Errors shown are statistical only. Systematic errors are estimated to be ~ 0.5 fm.

6 Summary

We have presented preliminary results on $p-p$, $\overline{p}-\overline{p}$ and $p-\overline{p}$ femtoscopy for Au + Au collisions at two energies: $\sqrt{s_{NN}} = 62$ GeV and $\sqrt{s_{NN}} = 200$ GeV per nucleon. Thanks to the large STAR dataset the data could be divided into three centrality classes. The $\overline{p}-\overline{p}$ and $p-\overline{p}$ correlation functions are measured and fitted for the first time. The measurements of proton femtoscopy are consistent within each centrality and collision energy. The proton and anti-proton source sizes were extracted with very good accuracy and were found to rise with the centrality of collisions for both energies. The results presented in this paper indicate that the residual correlations have a strong impact, more dominant in the non-identical hadron combinations. The extracted radii for central collisions follow a m_{T} dependence confirming that flow phenomena is affecting the different particle species. All radii from proton femtoscopy scale with $(\mathrm{d}N_{\mathrm{ch}}/\mathrm{d}\eta)^{1/3}$ variable as seen with mesonic resonances (Fig. 10).

Acknowledgements. We wish to thank the RHIC Operations Group and the RHIC Computing Facility at BNL, and the NERSC at LBNL for their support. Research supported by the Polish State committee for Scientific Research, grant 2P03B 05925. Research carried out within the scope of the ERG (GDRE): Heavy Ion at ultrarelativistic energies- a European Research Group comprising IN2P3/CNRS, Ecole des Mines de Nantes, Universite de Nantes, Warsaw University of Technology, JINR Dubna, ITEP Moscow and Bogolyubov Institute for Theoretical Physics NAS of Ukraine. We wish to especially thank Jan Pluta, Mike Lisa and Adam Kisiel for fruitful discussions and help.

References

1. E. Shuryak, Nucl. Phys. A **750**, 64 (2005)
2. E814/E877 Collaboration, J. Barrette et al., Phys. Rev. C **60**, 054 905 (1999)
3. NA44 Collaboration, H. Boggild et al., Phys. Lett. B **458**, 181 (1999)
4. NA49 Collaboration, H. Appelshauser et al., Phys. Lett. B **467**, 21 (1999)
5. FOPI Collaboration, R. Kotte et al., Eur. J. Phys. A **23**, 271 (2005)
6. R. Lednicky, Phys. Atom. Nucl. **67**, 72 (2004)
7. M. Lisa, S. Pratt, R. Soltz, U. Widemann, Ann. Rev. Nucl. Part. Sci. **55**, 357 (2005)
8. G. Goldhaber, S. Goldhaber, W.Y. Lee, A. Pais, Phys. Rev. **120**, 300 (1960)
9. G.I. Kopylov, M.I. Podgoretsky, Sov. J. Nucl. Phys. **15**, 219 (1972)
10. M. Gyulassy, S.K. Kauffamann, L.W. Willson, Phys. Rev. C **20**, 2267 (1979)
11. R. Lednicky, V.L. Lyuboshitz, Sov. J. Nucl. Phys. **35**, 770 (1982)
12. A. Kisiel, Nukleonika **49**, 81 (2004) suppl. 2
13. H. Gos, Accepted to Nukleonika (2006)
14. H. Gos, AIP Conf. Proc. **828**, 458 (2006)
15. G. Renault, Ph.D. thesis (2004)
16. A. Kisiel, T. Taluc, W. Broniowski, W. Florkowski, Comput. Phys. Commun. **174**, 669 (2006)
17. A. Kisiel, W. Broniowski, W. Florkowski, J. Pluta, Phys. Rev. C **73**, 064 902 (2006)
18. W. Broniowski, W. Florkowski, Phys. Rev. Lett. **87**, 272 302 (2001)
19. W. Broniowski, W. Florkowski, Phys. Rev. C **65**, 064 905 (2002)
20. A. Baran, W. Broniowski, W. Florkowski, Acta. Phys. Polon B **33**, 4235 (2002)
21. Z. Chajecki, Proc. Quark Matter 2005 Conf. (2006)
22. M.A. Lisa, F. Retiere, Phys. Rev. C **70**, 044 907 (2004)